ISSN 1674-1056
http://cpb.iphy.ac.cn
http://iopscience.iop.org/cpb
中国物理 B
Chinese Physics
中国物理
Chinese Physics B

Influence of helium on the evolution of irradiation-induced defects in tungsten: An object kinetic Monte Carlo simulation

Peng-Wei Hou(侯鹏伟), Yu-Hao Li(李宇浩), Zhong-Zhu Li(李中柱), Li-Fang Wang(王丽芳), Xingyu Gao(高兴誉), Hong-Bo Zhou(周洪波), Haifeng Song(宋海峰), and Guang-Hong Lu(吕广宏)
Citation: Chin. Phys. B, 2021, 30 (**8**): 086108. DOI: 10.1088/1674-1056/abf7ac
Journal homepage: http://cpb.iphy.ac.cn; http://iopscience.iop.org/cpb

What follows is a list of articles you may be interested in

Irradiation hardening behaviors of tungsten-potassium alloy studied by accelerated 3-MeV W^{2+} ions

Xiao-Liang Yang(杨晓亮), Long-Qing Chen(陈龙庆), Wen-Bin Qiu(邱文彬), Yang-Yi-Peng Song(宋阳一鹏), Yi Tang(唐毅), Xu-Dong Cui(崔旭东), Chang-Song Liu(刘长松), Yan Jiang(蒋燕), Tao Zhang(张涛), Jun Tang(唐军)
Chin. Phys. B, 2020, 29 (**4**): 046102. DOI: 10.1088/1674-1056/ab75cf

First-principles studies on carbon diffusion in tungsten

Chi Song(宋驰), Xiang-Shan Kong(孔祥山), C S Liu(刘长松)
Chin. Phys. B, 2019, 28 (**11**): 116106. DOI: 10.1088/1674-1056/ab4bb9

Room-temperature strong coupling between dipolar plasmon resonance in single gold nanorod and two-dimensional excitons in monolayer WSe_2

Jinxiu Wen(温锦秀), Hao Wang(汪浩), Huanjun Chen(陈焕君), Shaozhi Deng(邓少芝), Ningsheng Xu(许宁生)
Chin. Phys. B, 2018, 27 (**9**): 096101. DOI: 10.1088/1674-1056/27/9/096101

Label-free tungsten disulfide quantum dots as a fluorescent sensing platform for highly efficient detection of copper (II) ions

Xuan Zhao(赵宣), Da-Wei He(何大伟), Yong-Sheng Wang(王永生), Yin Hu(胡音), Chen Fu(付晨), Xue Li(李雪)
Chin. Phys. B, 2017, 26 (**6**): 066102. DOI: 10.1088/1674-1056/26/6/066102

Stability of concentration-related self-interstitial atoms in fusion material tungsten

Hong Zhang(张红), Shu-Long Wen(温述龙), Min Pan(潘敏), Zheng Huang(黄整), Yong Zhao(赵勇), Xiang Liu(刘翔), Ji-Ming Chen(谌继明)
Chin. Phys. B, 2016, 25 (**5**): 056102. DOI: 10.1088/1674-1056/25/5/056102

SPECIAL TOPIC — Ion beam modification of materials and applications

Influence of helium on the evolution of irradiation-induced defects in tungsten: An object kinetic Monte Carlo simulation*

Peng-Wei Hou(侯鹏伟)[1,2], Yu-Hao Li(李宇浩)[1,2,†], Zhong-Zhu Li(李中柱)[1,2], Li-Fang Wang(王丽芳)[3], Xingyu Gao(高兴誉)[3], Hong-Bo Zhou(周洪波)[1,2,‡], Haifeng Song(宋海峰)[3], and Guang-Hong Lu(吕广宏)[1,2]

[1] *Department of Physics, Beihang University, Beijing* 100191, *China*

[2] *Beijing Key Laboratory of Advanced Nuclear Materials and Physics, Beihang University, Beijing* 100191, *China*

[3] *Laboratory of Computational Physics, Institute of Applied Physics and Computational Mathematics, Beijing* 100088, *China*

(Received 5 March 2021; revised manuscript received 12 April 2021; accepted manuscript online 14 April 2021)

Understanding the evolution of irradiation-induced defects is of critical importance for the performance estimation of nuclear materials under irradiation. Hereby, we systematically investigate the influence of He on the evolution of Frenkel pairs and collision cascades in tungsten (W) via using the object kinetic Monte Carlo (OKMC) method. Our findings suggest that the presence of He has significant effect on the evolution of irradiation-induced defects. On the one hand, the presence of He can facilitate the recombination of vacancies and self-interstitial atoms (SIAs) in W. This can be attributed to the formation of immobile He-SIA complexes, which increases the annihilation probability of vacancies and SIAs. On the other hand, due to the high stability and low mobility of He-vacancy complexes, the growth of large vacancy clusters in W is kinetically suppressed by He addition. Specially, in comparison with the injection of collision cascades and He in sequential way at 1223 K, the average sizes of surviving vacancy clusters in W via simultaneous way are smaller, which is in good agreement with previous experimental observations. These results advocate that the impurity with low concentration has significant effect on the evolution of irradiation-induced defects in materials, and contributes to our understanding of W performance under irradiation.

Keywords: tungsten, helium, irradiation-induced defects, object kinetic Monte Carlo

PACS: 61.80.−x, 61.72.Cc, 61.72.−y **DOI:** 10.1088/1674-1056/abf7ac

1. Introduction

Tungsten (W), as a leading candidate for plasma facing materials (PFMs) in future fusion reactors, must withstand the extremely operational condition, including the high fluxes of hydrogen isotopes and helium plasma exposure ($\sim 10^{24}$ m^2·s^{-1}), an excessive heat load (up to 10 MW/m^2) and the irradiation of high-energy (14.1 MeV) fusion neutrons.[1–3] Specifically, in contrast to the near surface damage induced by plasma and heat, the neutron irradiation leads to the formation of radiation damage homogenously in the bulk system that dramatically affects the performance of W-PFMs, which has strong impact on the safety and economic efficiency of future fusion power plant.[4–7] Microscopically, neutron radiation damage is mainly originated from the displacement damage, producing numerous irradiation-induced defects in materials, such as vacancies, self-interstitial atoms (SIAs) and their clusters. These defects will interact with each other and intrinsic defects/impurities, which should be responsible for the microstructure evolution and performance variation of materials under neutron irradiation.[8–13] Therefore, it is of great importance to accurately determine the evolution of irradiation-induced defects in nuclear materials.

As the production of (n, α) transmutation reaction and deuterium-tritium (D-T) fusion reaction, helium (He) is a typical impurity in nuclear environment and has significant effects on the mechanical properties of materials.[14,15] For example, the presence of He can significantly degrade the mechanical properties of fission materials, known as high-temperature He embrittlement.[16–18] Interestingly, not only the mechanical properties, but also the evolution of irradiation-induced defects in W is significantly affected by He addition. For example, using the positron annihilation lifetime spectroscopy, Thompson *et al.*[19] determined the number and size of vacancy-type defects in W after the irradiation of high-energy heavy ions (1 MeV W) and low-energy ($\sim$ 30 eV) He plasma. In comparison with the irradiation of W ions only, the subsequent irradiation of He plasma substantially increases the positron lifetime of materials, which shows that the presence of He facilitates the clustering of vacancies in W. Similar results were also observed by Getto *et al.*[20] and Ayanoglu *et al.*[21] Besides the clustering effects, the He addition may also enhance the recombination of irradiation-induced defects. For exam-

*Project supported by the Science Challenge Project (Grant No. TZ2018002), the National Natural Science Foundation of China (Grant No. 11905135), and the National MCF Energy R&D Program of China (Grant No. 2018YFE0308103).

†Corresponding author. E-mail: yuhaoli@buaa.edu.cn

‡Corresponding author. E-mail: hbzhou@buaa.edu.cn

ple, Sun *et al.*[22] investigated the total D retention in damaged W (6.4 MeV Fe ions irradiation alone and Fe+He ions irradiation simultaneously). It is found that the D retention after Fe ions irradiation alone is about 17% higher than that after dual ions irradiation, which can be attributed to the reduction of vacancy numbers (known as the strong trapping sites for D), implying the promoting effect of He on the recombination of vacancies and SIAs. This is also supported by EI-Atwani *et al.*,[23] in which the damage levels (density and average area/size of dislocation loop and cavity, and total change in volume) in W at 1223 K after sequential (He irradiation followed by Kr implantation and vice-versa) and simultaneous (He+Kr dual beam) irradiation were identified. Specifically, the smallest damage in W was observed after simultaneous irradiation, which can be rationalized by the enhancing effect of He implantation on the recombination of Kr generated defects. These experiments demonstrated the critical role of He on the evolution of irradiation-induced defects in W, while the underlying mechanism remains to be clarified.

Multi-scale simulation is an effective method to explore the defects evolution in materials.[2,24–26] Density functional theory (DFT) calculations shows that there is a strong attractive interaction between He and vacancy in W with the binding energy of ~ 4.57 eV, indicating the formation of He-vacancy (He-V) clusters.[27] The high stable and immobile He-V complexes can serve as the trapping center for subsequent He and vacancy, leading to the growth of He-V clusters.[28–30] At the same time, the binding energy of He with SIA in W can reach up to ~ 1 eV, and increases with the increasing of SIA numbers.[31–33] Different from the immobile He-V complexes, the diffusion energy barrier of specific He-SIA complexes (e.g., He_1-SIA_1 and He_1-SIA_2) is also low, which suggests the high mobility of these He-SIA complexes in W at moderate temperature.[34] Based on these DFT results as input, many efforts have been made to determine the evolution of He and defects in W via using molecular dynamics (MD) and kinetic Monte Carlo (KMC) methods.[35–39] However, previous large-scale simulations are mainly focused on the behaviors of He in W (e.g., He retention and He bubble formation), and thus the influence of He on the evolution of irradiation-induced defects is not still clear.

In the present work, we will systematically investigate the influence of He on the evolution of irradiation-induced defects (Frenkel pairs or cascades) in W via using object KMC (OKMC) method. The density and size of He-V complexes as well as the recombination of vacancy and SIA will be analyzed in detail to determine the He effects. It is found that the presence of He enhances the recombination of Frenkel pairs (i.e., vacancies and SIAs) at high temperature, which can be attributed to the formation of immobile He-SIA complexes. Besides, owing to the strong attraction of He-V complexes, the He addition effectively suppresses the mobility of vacancies, and thus kinetically inhibits the formation of large vacancy clusters in W. By comparing the surviving defects in W after sequential simulation (collision cascades followed by He implantation) with that under simultaneous (collisions cascades plus He implantation) way, we find that the average size (number) of vacancy clusters at 1223 K under sequential method is larger (lower) than that under simultaneous method. This trend is in good agreement with experiments. These results will deepen our understanding of the microstructure evolutions and properties of W-PFMs under neutron irradiation.

2. Computation methods

Our OKMC simulations were performed in a self-developed code, which is suitable to investigate the defects evolution in nuclear materials.[40] Within the OKMC framework, all defects (i.e., vacancy, SIA, He and their complexes) are regarded as the objects at specific position with postulated reaction radii. In OKMC simulations, there are two different types of process that may occur, including the thermal-activated event and non-thermal-activated event. The former includes the defects migration and dissociation, which are selected randomly based on their probabilities (it is calculated by Arrhenius formula and thus dependent on the activation energy and attempt frequency). Once a thermal-activated event is selected, the types and positions of objects are updated, and the simulation time is calculated by residence time algorithm. As for the non-thermal-activated event, it contains the defects clustering and annihilation, and is only related to the distance between two objects and occurred spontaneously without time increment. The detailed information of our OKMC model are described in Refs. [34,40,41] and references therein.

The OKMC simulation was carried out to determine the influence of He on the evolution of irradiation-induced defects in W. As known to all, the results of OKMC simulation are directly related to the parameters. Here, the binding energies of pure vacancy clusters (V_n) were taken from the publications by Huang *et al.*,[42] while the binding energies of pure SIA clusters (SIA_m) and He clusters (He_k) were obtained from the publication by Becquart *et al.*[43] For He-V complex, the binding energies reported by Valles *et al.*[37] (for small He_kV_n clusters, $k \leq 4$ and $n \leq 4$) and Li *et al.*[44] (for large He_kV_n complexes, $k > 4$ or $n > 4$) were employed. These values were in good agreement with previous DFT results.[43] Moreover, the binding energies of He with SIA_1, SIA_2 and SIA_3 were parameterized by Ma *et al.*[34] and You *et al.*[33] As for larger He-SIA clusters, their binding energies were estimated by power law based on the reported DFT data

$$E_b = -2.31\,e^{-n/4.28} + 3.0, \tag{1}$$

where E_b is the binding energy of He and SIA clusters and n is the number of SIA in He-SIA clusters.

Concerning migration parameters, the diffusion energy barriers and attempt frequency of a single vacancy and small vacancy clusters ($n < 4$) were taken from Li *et al.*[41] and Becquart *et al.*,[43] while the large vacancy clusters ($n \geq 4$) were considered immobile. The kinetic parameters of pure SIA clusters and He clusters were also taken from Becquart *et al.*[43] For the mixed He-V and He-SIA complexes, their mobilities are neglected owing to the high diffusion energy barrier, except for He_1-SIA_1 and He_1-SIA_2 (it has been reported that the diffusion energy barrier of He_1-SIA_1 and He_1-SIA_2 is 0.38 and 0.64 eV, respectively).[34]

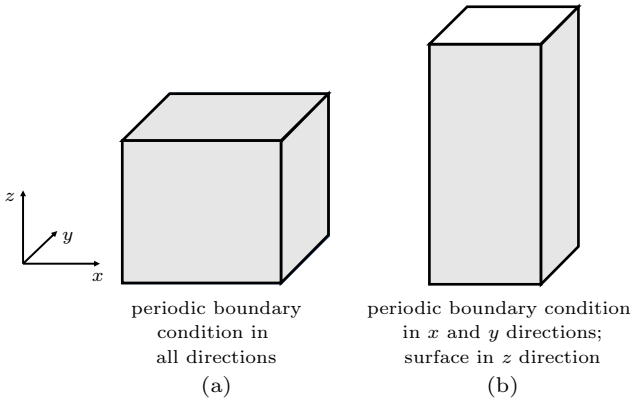

Fig. 1. The simulation box for OKMC calculations, (a) injection of Frenkel pairs and (b) injection of collision cascades.

Figure 1 shows the simulation boxes selected in our calculations. Notably, similar with previous studies,[45–47] there are no real atomic lattices in OKMC simulation. As seen in Fig. 1(a), a near-club simulation cell with trilateral length of $169 \times 173 \times 178 a_0^3$ was chosen to explore the influence of He on the evolution of Frenkel pairs in bulk W. In this case, the periodic boundary condition (PBC) in all three directions was employed. Namely, the defects will return to the simulation box through the opposite surface if it reaches the boundary. Further, when the collision cascades were injected, a simulation box with trilateral length of $99 \times 100 \times 315 a_0^3$ was selected. Correspondingly, the PBC was used in x/y direction, while the absorbing boundary condition was used in z direction to simulate a slab system. Here, the absorbing boundary means that the boundary is considered as perfect sink, i.e., all defects (vacancies, SIAs and He atoms) that reach the boundary will be removed from the simulation box instantly. Such boundary condition can be employed to simulate the defects evolution in a slab or nanostructured materials (high grain boundary density), and hence has been widely used in previous OKMC studies.[46,48,49] Notably, in order to describe the absorption of defects in grain boundaries (GBs), the sink strength was also taken into account and expressed as[50–52]

$$k^2 = \begin{cases} 15/R_{GB}^2, & \text{for 1D migration defects,} \\ 14.4/R_{GB}^2, & \text{for 3D migration defects,} \end{cases} \quad (2)$$

where k^2 is the effective sink strength for migrating objects, and R_{GB}^2 is the grain radius. In our calculation, a grain radius of 2 μm was chosen, corresponding to the typical grain sizes in W.[53] For each case, OKMC simulation was repeated twenty times independently and the average results were provided in the following sections.

3. Results and discussion

3.1. Influence of He on the evolution of Frenkel pairs in W

The Frenkel pairs are the most common irradiation-induced defects in materials and their behaviors should be significantly affected by He addition, because of the strong interactions of He with vacancies and SIAs. To show the influence of He on the behaviors of Frenkel pairs, we firstly determine the evolution of Frenkel pairs in pure W and W-He system (1 and 10 appm He). For reference, the concentration of transmutation-induced He in W can reach up to 2 appm and 3.36 appm after three and five years under power-plant condition, respectively.[54] Here, three different temperatures are considered, including 600 K (on-set temperature for vacancy migration), 1050 K (peak swelling temperature[55]) and 1400 K (recrystallization temperature[56]). The concentration of the Frenkel pairs is set to be 100 appm, and all defects are introduced randomly and simultaneously. To mimic the cascade effect, the fraction of different vacancy clusters is also considered, i.e., 65% V_1, 20% V_3 and 15% V_4 (approximated as stable vacancy clusters), which is consistent with the previous study.[57]

As the key event of self-healing process, the recombination of the Frenkel pairs is directly related to the ability of materials to resist irradiation damage. Thus, we examine the recombination rate of the Frenkel pairs in W with and without He. Here, the recombination rate (R) at specific time (t_1) is defined as

$$R(t_1) = \frac{N_{re}(t_1 + \Delta t) - N_{re}(t_1)}{\log(t_1 + \Delta t) - \log(t_1)}, \quad (3)$$

where $N_{re}(t_1)$ is the total recombination numbers of the Frenkel pairs at t_1. Figure 2 shows the recombination rate of vacancies and SIAs in pure W and W-He system at 1050 K as a function of simulation time. Obviously, the variation of recombination rate of the Frenkel pairs in pure W appears only one distinct peak at 10^{-9} s, and the recombination tail can reach up to 10^{-4} s. In this case, the annihilation of vacancies and SIAs should be attributed to the migration of SIAs (with extremely low migration energy barriers, < 0.013 eV) that eliminates vacancies in W. After that, the recombination rate is almost equal to zero, as displayed in Fig. 2. The reason is that GBs can serve as the trapping center for fast-moving SIAs leading to the low recombination probability in W.

As seen in Fig. 2, the He addition can dramatically affect the recombination of the Frenkel pairs in W. Different from a single peak of recombination rate in pure W, there are two distinct peaks for the recombination of the Frenkel pairs in W-He system. The first peak also appears at 10^{-9} s with a tail up to 10^{-4} s in W-He system, but the corresponding recombination rate in 10^{-8}–10^{-4} s is slightly lower than that in pure W, as displayed in Fig. 2. This can be attributed to the attractive interaction between He and SIAs, which reduces the mobility of SIAs and thus the recombination rate. Specifically, the unexpected second peak of recombination rate of the Frenkel pairs in W-He system appears at 10^{-1}–10^{0} s with a tail up to 10^{3} s. This can be rationalized by the motion of vacancy and small vacancy clusters, which eliminate the immobile He-SIA complexes in W. After that, the recombination rate in W-He system converges to zero. Since the overall recombination number (the area under the curve of recombination rate) in W-He system is higher than that in pure W, the He addition enhances the recombination of the Frenkel pairs. Such promoting effect is consistent with our previous study, in which the evolution of the Frenkel pairs in W-He system at room temperature (300 K) was determined.[34] However, it is important to note that the enhancing effect of He on the recombination of the Frenkel pairs in W at room temperature is originated from the collaborative motion of small He-SIA complexes, which is totally different from the cases in the present work.

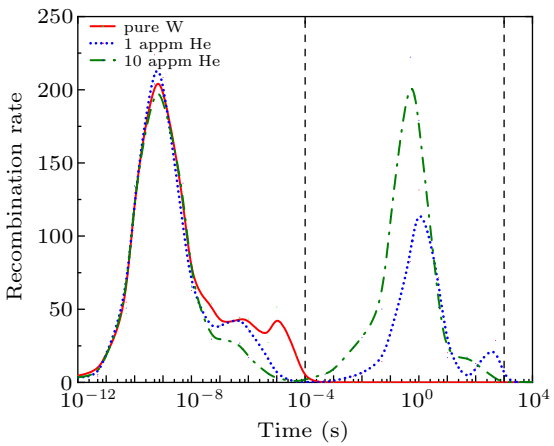

Fig. 2. The recombination rate of the Frenkel pairs in pure W and W-He systems at 1050 K.

Next, we analyze the number and type of remaining defects in W with and without He. Figure 3(a) shows the size distribution of remaining vacancy clusters in pure W and W-He system at 1050 K. For the case of pure W, the number of single vacancy and small vacancy clusters ($n < 30$) are extremely low (< 1), while the number of large vacancy clusters ($n > 50$) can reach nearly up to 5. This means that the great majority of vacancies is aggregated, corresponding to the formation of large vacancy clusters, which can be attributed to the high stability of large vacancy clusters. However, the distribution of vacancy clusters in W-He system is obviously different from that in pure W. As seen in Fig. 3(a), the presence of He significantly reduces the number of large vacancy clusters in W, while the number of single vacancies increases substantially. For example, the number of large vacancy clusters ($n > 50$) reduces from ~ 5 in pure W, to ~ 2 with 1 appm He and ~ 0 with 10 appm He. In contrast, the number of single vacancy increases from ~ 1 in pure W, to 8 with 1 appm He and 52 with 10 appm He. These results suggest that the He atoms can effectively suppress the formation of large vacancy clusters. As demonstrated in previous atomic simulations,[27,58] the He addition significantly increases the migration energy barrier of vacancies in W, since the binding energy (~ 4.57 eV) between He and vacancy is much higher than the migration energy barrier (< 1.70 eV) of small vacancy clusters ($n \leq 3$).[48,59,60] Therefore, the presence of He reduces the mobility of small vacancy clusters in W, and hence suppresses the growth of vacancy clusters kinetically.

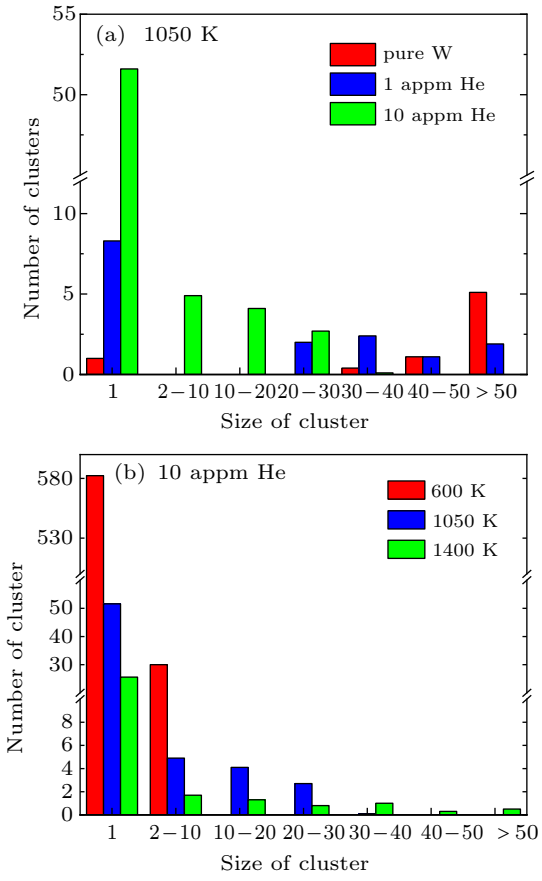

Fig. 3. Number of vacancy clusters in pure W and W-He system as a function of cluster sizes, (a) with different He concentration at 1050 K and (b) with 10 appm He at different temperatures.

In order to determine the influence of temperature on the evolution of the Frenkel pairs, we further analyze the size distribution of vacancy clusters in W with 10 appm He at different temperature. As displayed in Fig. 3(b), the temperature has significant effects on the distribution of remaining vacancy clusters in W-He system. When the temperature is 600 K, only the single vacancy and small vacancy clusters ($2 \leq n \leq 10$) are

observed. This can simply attribute to the low mobility of vacancy and vacancy clusters at 600 K (on-set temperature for vacancy migration), reducing the probability for the formation of large vacancy clusters. Nevertheless, with the increasing of temperature, the number of single vacancy reduces from 582 at 600 K to 26 at 1400 K, while that of large vacancy clusters ($n > 30$) increases from ~ 0 at 600 K to 2 at 1400 K. The formation of large vacancy clusters at high temperature ($\sim$ 1400 K) should be originated from the dissociation of He-V complexes and small vacancy clusters, leading to the formation of single vacancy, which eventually enhances the formation of large vacancy clusters.

3.2. Influence of He on the evolution of defects in pre-irradiated W

The primary damaged structures induced by high-energy neutron/ion irradiation in materials are collision cascades, instead of the Frenkel pairs. Hence, similar with the previous experiment,[23] we further investigate the influence of He on the evolution of defects in pre-irradiated W. In this case, the OKMC simulation can divided into two stages. In the first stage, only the collision cascades are injected into the simulation box. Here, the primary knock-on atom energy of 200 keV is selected and the corresponding cascades debris are obtained through rigorous MD simulations.[61] Besides, the standard NRT model has been employed to estimate the injection rate of cascades.[62] In order to compare with the previous experiment,[23] the dose rate of cascade is set to be 0.0016 dpa/s and the total irradiation dose can reach up to 0.25 dpa. Then, in the second stage, the He irradiation (one He atom plus four Frenkel pairs) is occurred and the corresponding flux is 3.9×10^{12} cm^{-2}·s^{-1} with total fluence of 3.1×10^{15} cm^{-2}. All cascades and He implantation are introduced randomly.

Figure 4 shows the average size and number of vacancy clusters as a function of irradiation dose in W after cascade damage. Although the variation trends of vacancy clusters are similar in different temperature, the temperature has significant effects on the number and type of vacancy clusters in W. At 600 K, both average size and number of vacancy clusters increases sharply (or even instantly) at low irradiation dose (< 0.013 dpa). After that, the average size of vacancy clusters increases slightly in the range of 2 to 2.5, while the number of vacancy clusters monotonically increases with the increasing of irradiation dose, from 7524 at 0.013 dpa to 30952 at 0.25 dpa. This can be simply understood by the low mobility of vacancy in W at 600 K, which kinetically restrains the growth of vacancy clusters. As shown in Figs. 4(b) and 4(c), even though the irradiation dose is higher than 0.15 dpa, the average size of vacancy clusters at 1050 K and 1400 K also increases with the increasing of irradiation dose, and reach up to 84.1 and 145.6, respectively. These values are 1–2 magnitudes higher than that at 600 K, indicating the formation of large vacancy clusters at high temperature. Accordingly, due to the aggregation of vacancies at high temperature, the number of vacancy clusters at 600 K is much higher than that at 1050 K and 1400 K, as seen in Fig. 4.

Then, based on the cascade damage obtained above, we further analyze the defects information in W after He irradiation (He plus Frenkel pairs in the second stage). For reference, the cases without He irradiation (only Frenkel pairs are inserted in the second stage) are also presented. As illustrated in Fig. 5(a), the influence of He on the further evolution of cascade damage in W at 600 K is almost negligible, since

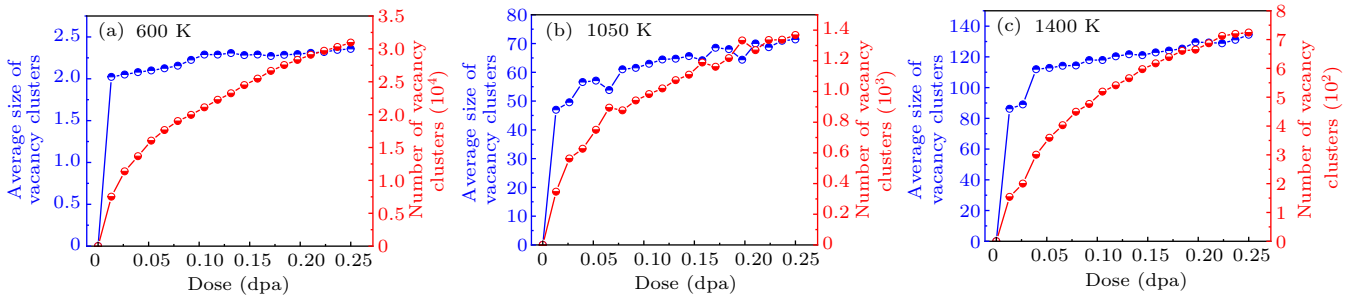

Fig. 4. The average size and number of vacancy clusters in W as a function of dpa at (a) 600 K, (b) 1050 K, and (c) 1400 K.

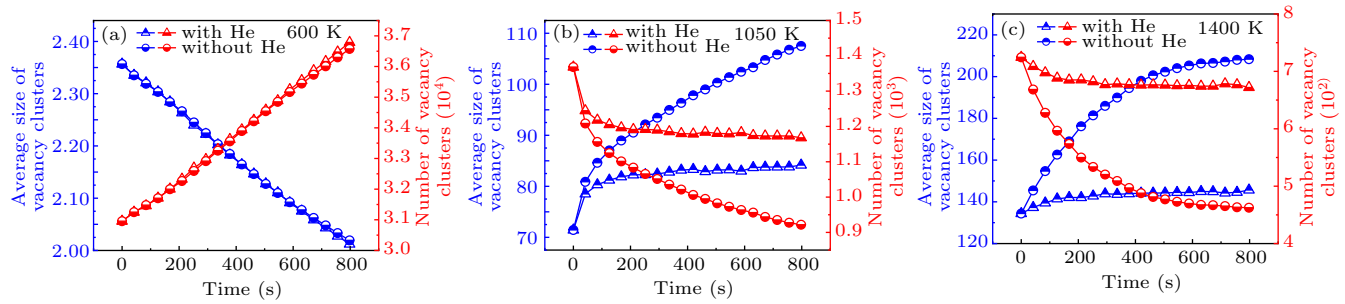

Fig. 5. The average size and number of vacancy clusters as a function of simulation time at (a) 600 K, (b) 1050 K, and (c) 1400 K. The case without He corresponds to the results that only Frenkel pairs are inserted.

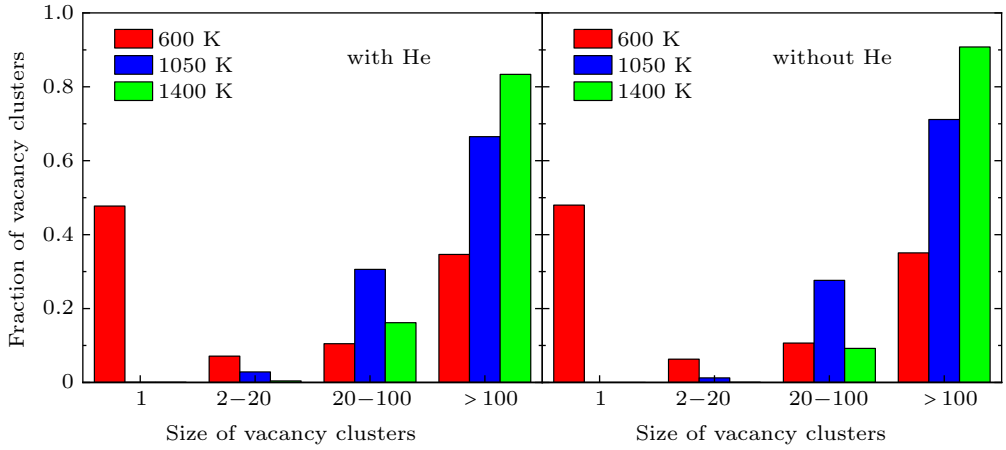

Fig. 6. The fraction of different sizes of surviving vacancy clusters in W at different temperature, (a) with and (b) without He implantation. The fraction of vacancy clusters is calculated by the ratio of the number of vacancies in the specific clusters to the total number of vacancies, see Eq. (4).

both the number and average size of vacancy clusters after He implantation are consistent with that after injection of the Frenkel pairs only (without He). In this case, the average size of vacancy clusters decreases with the increasing of simulation time, while the number of vacancy clusters increases. However, when the temperature is increased to 1050 K, the results are substantially different. As displayed in Fig. 5(b), although the average size (number) of vacancy clusters increases (decreases) with the increasing of simulation time regardless of He addition, the presence of He can significantly reduce the growth rate of vacancy clusters and hence increase the number of remaining vacancy clusters. For example, the average size and number vacancy clusters are 84.2 and 1167.6 after He irradiation, while are 106.2 and 934.8 without He addition, respectively. Similar results are also observed at 1400 K, as demonstrated in Fig. 5(c).

Figure 6 shows the fraction of different vacancy clusters in W after He implantation (with He) and injection of the Frenkel pairs only (without He). The fraction of vacancy clusters is defined as

$$F_i = [i(\mathrm{He}_k\mathrm{V}_i) + i(V_i)] \Big/ \left[\sum_n n(\mathrm{He}_k\mathrm{V}_n) + \sum_n n(V_n)\right], \quad (4)$$

where $(\mathrm{He}_k\mathrm{V}_n)$ is the number of $\mathrm{He}_k\mathrm{V}_n$ clusters. As displayed in Fig. 6, the fraction of vacancy clusters at 600 K is almost independent on He addition, suggesting the negligible effects of He on the evolution of vacancy clusters. This can be rationalized by the low mobility of vacancies in W at 600 K, which limits the further evolution of vacancy clusters. Nevertheless, the fraction of large vacancy clusters at high temperature is substantially reduced by He addition, and this influence is enhanced with the increasing of temperature. For example, the large vacancy clusters ($n > 100$) take up to 71.2% and 90.8% for the total number of remaining vacancies at 1050 K and 1400 K without He addition, while it is reduced to 66.5% and 83.4% with He irradiation. Such suppressing effect of He on the aggregation of vacancies should be attributed to the formation of He-V complexes, which reduces the mobility of vacancies in W.

3.3. Synergistic evolution of He and collision cascades in W

In a fusion environment, W-PFMs will be exposed by He and high-energy neutrons simultaneously, which should be different from the displacement cascades and He irradiation in sequential way. Thus, to accurately describe the synergistic effects of He and irradiation-induced defects, we inject the He atoms and collision cascades into the simulation box in a simultaneous way. Similar with the previous experiment,[23] the simulation time is 800 s and the temperature is 1223 K. The dose rate of cascades is set to be 0.000313 dpa/s to achieve the same final irradiation dose (in comparison with the results in sequential way). For reference, the defects evolutions in sequential method at 1223 K are also presented. Other conditions are the same as the sequential simulations in Section 3.2.

Figure 7 shows the average size and number of vacancy clusters in W as a function of dpa/fluence at 1223 K. For the sequential irradiation, it is found that both average size and number of vacancy clusters will increase with the increasing of dpa and a nearly constant during He implantation at 1223 K, which is basically consistent with that at 1050 K and 1400 K (see Figs. 4 and 5). The similar variation trend is also observed for the simultaneous irradiation in W at 1223 K, as illustrated in Fig. 7(b). However, it is important to note that the average size of vacancy clusters after sequential irradiation is much higher than that after simultaneous irradiation at the same temperature, while the number of vacancy clusters after sequential irradiation is smaller than that after simultaneous irradiation. For example, the average size and number of vacancy clusters after irradiation can reach up to $\sim$ 117.7 and 831.8 in sequential method, while it is 90.2 and 1159.8 in simultaneous method, respectively. These results are in good

agreement with the previous experiment,[23] in which the average size of cavity in W after simultaneous irradiation (1 MeV Kr plus 16 keV He dual beams) is slightly smaller than that after sequential irradiation (Kr irradiation followed by He implantation), and vice-versa for the cavity numbers.

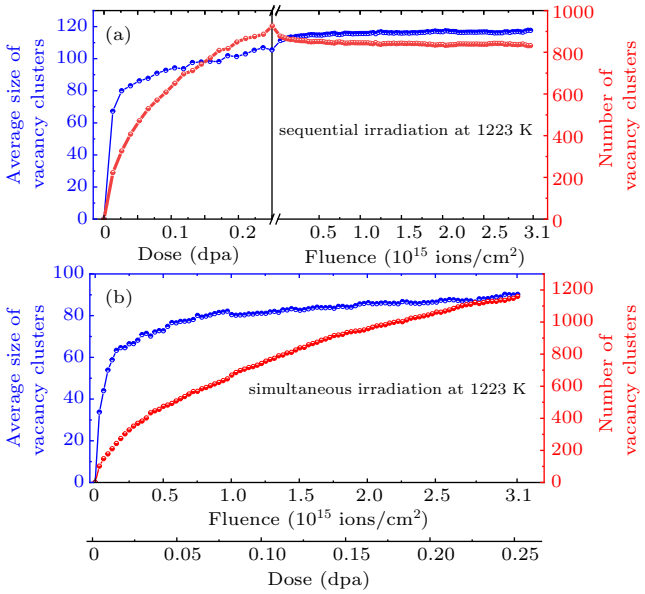

Fig. 7. The average size and number of vacancy cluster in W as a function of dpa and fluence at 1223 K after (a) sequential and (b) simultaneous irradiation.

Above results clearly demonstrate that the suppressing effect of He on the formation of large vacancy clusters under simultaneous irradiation is stronger than that under sequential irradiation in W at 1223 K. However, as discussed in Section 3.2, temperature is a key factor to significantly affect the evolution of cascades. Here, we further investigate the influence of temperatures on the defects evolution under simultaneous and sequential irradiation, respectively. As shown in Fig. 8, the average size of remaining vacancy clusters in W is directly related to the simulation temperature. With the increasing temperature, the average size monotonically increases, regardless of irradiation method (simultaneously or sequentially). More importantly, the relative sizes of vacancy clusters under simultaneous and sequential irradiation are also dependent on the temperature, as displayed in Fig. 8. When the temperature is lower than 1050 K, the average size of vacancy clusters after sequential irradiation is smaller than that under simultaneous irradiation. However, once the temperature is higher than 1050 K, the relative size of vacancy clusters appears an opposite trend, in which the average size after sequential irradiation is larger than that under simultaneous irradiation. For example, the average size of vacancy clusters after simultaneous and sequential irradiation in W at 800 K is 49 and 32.8, while at 1400 K is 100.1 and 145.5, respectively.

Such intriguing and temperature-dependent relative size of vacancy clusters in W should be originated from the interaction between He and vacancies. On the one hand, due to the strong attractive interaction between He and vacancies, the He addition can stabilize the small vacancy clusters, especially for V_2 and V_3 clusters (since pure V_2 and V_3 are energetically unstable in W). These complexes can serve as nucleation sites for subsequent vacancies, enhancing the growth of vacancy clusters, which increases the average size of vacancy clusters in W after simultaneous irradiation at 800 K. On the other hand, the formation of He-V complexes can significantly suppress the mobility of vacancies, which inhibits the formation of large vacancy clusters kinetically and hence reduces the average size of vacancy clusters in W at 1400 K.

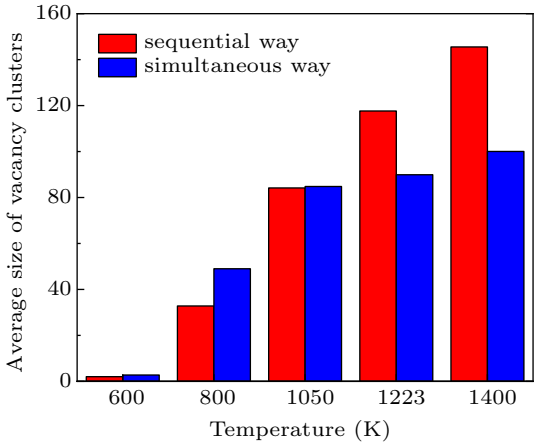

Fig. 8. The average size of vacancy clusters in W after sequential and simultaneous irradiation at different temperature.

4. Conclusion

In the present work, we have systematically investigated the influence of He on the evolution of irradiation-induced defects (corresponding to the high-energy particles irradiation) in W by using the OKMC method. Both the Frenkel pairs and collision cascades obtained by MD simulations are employed as input, and the temperature ranges from 600 K to 1400 K. Notably, two different methods of defects injection are considered, i.e., the sequential method (collision cascades followed by He implantation) and the simultaneous method (collision cascades plus He implantation). According to our simulation, the recombination of the Frenkel pairs is enhanced by He addition, which should be attributed to the pinning effects of He on SIAs in W. The formation of immobile He-SIA complexes decreases the absorption probability of SIAs into GBs and can be eliminated by mobile vacancies, which enhances vacancy-SIA recombination and reduces the number of surviving defects. Moreover, owing to the strong attractive interaction between He and vacancies, the He addition significantly reduces the mobility of vacancies in W, and thus suppresses the formation of large vacancy clusters. Specifically, by analyzing the defects evolution after sequential and simultaneous irradiation, we found that the average size of vacancy clusters after sequential way is much larger than that after simultaneous method at 1223 K, and vice-versa for the vacancy cluster

numbers. These results are well consistent with experimental observations. Our calculation not only provides a good reference to understand the influence of He on defects evolution during high-energy particles irradiation, but also contributes to the performance estimation of W-PFMs.

References

[1] Bloom E E, Zinkle S J and Wiffen F W 2004 *J. Nucl. Mater.* **329** 12
[2] Zinkle S J 2005 *Phys. Plasmas* **12** 058101
[3] Yin H, Wang J, Guo W G, Cheng L and Lu G H 2019 *Tungsten* **1** 132
[4] Hu X X, Koyanagi T, Fukuda M, Kumar N A P K, Snead L L, Wirth B D and Katoh Y 2016 *J. Nucl. Mater.* **480** 235
[5] Li Y G, Zheng Q R, Wei L M, Zhang C G and Zeng Z 2020 *Tungsten* **2** 34
[6] Hu X X, Koyanagi T, Fukuda M, Katoh Y, Snead L L and Wirth B D 2016 *J. Nucl. Mater.* **470** 278
[7] Song Y Y P, Qiu W B, Chen L Q, Yang X L, Deng H, Liu C S, Zhang K and Tang J 2020 *Chin. Phys. B* **29** 105202
[8] Hu L, Wirth B D and Maroudas D 2017 *Appl. Phys. Lett.* **111** 081902
[9] Zhou H B, Liu Y L, Jin S, Zhang Y, Luo G N and Lu G H 2010 *Nucl. Fusion* **50** 025016
[10] El-Atwani O, Aydogan E, Esquivel E, Efe M, Wang Y Q and Maloy S A 2018 *Acta Mater.* **147** 277
[11] Bonny G, Castin N, Bakaev A, Sand A E and Terentyev D 2020 *Comp. Mater. Sci.* **181** 109727
[12] Sand A E, Nordlund K and Dudarev S L 2014 *J. Nucl. Mater.* **455** 207
[13] Zhang H, Wen S L, Pan M, Huang Z, Zhao Y, Liu X and Chen J M 2016 *Chin. Phys. B* **25** 056102
[14] Katoh Y, Snead L L, Garrison L M, Hu X, Koyanagi T, Parish C M, Edmondson P D, Fukuda M, Hwang T, Tanaka T and Hasegawa A 2019 *J. Nucl. Mater.* **520** 193
[15] Abernethy R G 2017 *Mater. Sci. Tech.* **33** 388
[16] Zinkle S J and Busby J T 2009 *Mater. Today* **12** 12
[17] Zinkle S J and Was G S 2013 *Acta Mater.* **61** 735
[18] Gilbert M R, Dudarev S L, Zheng S, Packer L W and Sublet J C 2012 *Nucl. Fusion* **52** 083019
[19] Thompson M, Drummond D, Sullivan J, Elliman R, Kluth P, Kirby N, Riley D and Corr C S 2018 *Nucl. Fusion* **58** 066010
[20] Getto E, Jiao Z, Monterrosa A M, Sun K and Was G S 2015 *J. Nucl. Mater.* **462** 458
[21] Ayanoglu M and Motta A T 2018 *J. Nucl. Mater.* **510** 297
[22] Sun F, Nakata M, Lee S E, Zhao M, Wada T, Yamazaki S, Koike A, Kondo S, Hinoki T, Hara M and Oya Y 2020 *J. Nucl. Mater.* **533** 152122
[23] El-Atwani O, Cunningham W S, Trelewicz J R, Li M, Wirth B D and Maloy S A 2020 *J. Nucl. Mater.* **538** 152150
[24] Nordlund K, Bjorkas C, Ahlgren T, Lasa A and Sand A E 2014 *J. Phys. D-Appl. Phys.* **47** 224018
[25] Valles G, Cazalilla A L, Gonzalez C, Martin-Bragado I, Prada A, Iglesias R, Perlado J M and Rivera A 2015 *Nucl. Instrum. Meth. B* **352** 100
[26] Derlet P M, Nguyen-Manh D and Dudarev S L 2007 *Phys. Rev. B* **76** 054107
[27] Zhou H B, Liu Y L, Jin S, Zhang Y, Luo G N and Lu G H 2010 *Nucl. Fusion* **50** 115010
[28] You Y W, Li D D, Kong X S, Wu X B, Liu C S, Fang Q F, Pan B C, Chen J L and Luo G N 2014 *Nucl. Fusion* **54** 103007
[29] Boisse J, Domain C and Becquart C S 2014 *J. Nucl. Mater.* **455** 10
[30] Zhou H B, Wang J L, Jiang W, Lu G H, Aguiar J A and Liu F 2016 *Acta Mater.* **119** 1
[31] Bakaev A, Grigorev P, Terentyev D, Bakaeva A, Zhurkin E E and Mastrikov Y A 2017 *Nucl. Fusion* **57** 126040
[32] You Y W, Sun J J, Wu X B, Xu Y C, Zhang T, Hao T, Fang Q F and Liu C S 2019 *Nucl. Fusion* **59** 026002
[33] You Y W, Sun J J, Kong X S, Wu X B, Xu Y C, Wang X P, Fang Q F and Liu C S 2020 *Phys. Scripta* **95** 075708
[34] Ma F F, Hou P W, Li Z Z, Li Y H, Niu Y Z, Ma H Z, Ren Q Y, Gao F, Lu G H and Zhou H B, to be published
[35] Sandoval L, Perez D, Uberuaga B P and Voter A F 2015 *Phys. Rev. Lett.* **114** 105502
[36] Gao E and Ghoniem N M 2018 *J. Nucl. Mater.* **509** 577
[37] Valles G, Gonzalez C, Martin-Bragado I, Iglesias R, Perlado J M and Rivera A 2015 *J. Nucl. Mater.* **457** 80
[38] Wang J, Dang W, Liu D and Guo Z 2020 *Chin. Phys. B* **29** 093101
[39] Li F B, Ran G, Gao N, Zhao S Q and Li N 2019 *Chin. Phys. B* **28** 085203
[40] Li Z Z, Li Y H, Ren Q Y, Ma F F, Yue F Y, Zhou H B and Lu G H 2020 *Materials* **13** 3375
[41] Li Z Z, Li Y H, Terentyev D, Castin N, Bakaev A, Bonny G, Yang Z C, Gao F, Lu G H and Zhou H B, to be published
[42] Huang G Y, Juslin N and Wirth B D 2016 *Comp. Mater. Sci.* **123** 121
[43] Becquart C S, Domain C, Sarkar U, DeBacker A and Hou M 2010 *J. Nucl. Mater.* **403** 75
[44] Li X C, Liu Y N, Yu Y, Luo G N, Shu X L and Lu G H 2014 *J. Nucl. Mater.* **451** 356
[45] Christiaen B, Domain C, Thuinet L, Ambard A and Legris A 2020 *Acta Mater.* **195** 631
[46] Panizo-Laiz M, Diaz-Rodriguez P, Rivera A, Valles G, Martin-Bragado I, Perlado J M, Munnik F and Gonzalez-Arrabal R 2019 *Nucl. Fusion* **59** 086055
[47] Martin-Bragado I, Rivera A, Valles G, Gomez-Selles J L and Caturla M J 2013 *Comput. Phys. Commun.* **184** 2703
[48] Valles G, Panizo-Laiz M, Gonzalez C, Martin-Bragado I, Gonzalez-Arrabal R, Gordillo N, Iglesias R, Guerrero C L, Perlado J M and Rivera A 2017 *Acta Mater.* **122** 277
[49] Becquart C S, Barthe M F and De Backer A 2011 *Phys. Scripta* **T145** 014048
[50] Malerba L, Becquart C S and Domain C 2007 *J. Nucl. Mater.* **360** 159
[51] Castin N, Bakaev A, Bonny G, Sand A E, Malerba L and Terentyev D 2017 *J. Nucl. Mater.* **493** 280
[52] Roth J, Tsitrone E, Loarte A, Loarer T, Counsell G, Neu R, Philipps V, Brezinsek S, Lehnen M, Coad P, Grisolia C, Schmid K, Krieger K, Kallenbach A, Lipschultz B, Doerner R, Causey R, Alimov V, Shu W, Ogorodnikova O, Kirschner A, Federici G, Kukushkin A, Force E P T, Team I P, Energy F and DIV I S 2009 *J. Nucl. Mater.* **390-391** 1
[53] Alimov V K, Tyburska-Püschel B, Lindig S, Hatano Y, Balden M, Roth J, Isobe K, Matsuyama M and Yamanishi T 2012 *J. Nucl. Mater.* **420** 519
[54] Gilbert M R and Sublet J C 2011 *Nucl. Fusion.* **51** 043005
[55] Matolich J, Nahm H and Moteff J 1974 *Scripta Metallurgica* **8** 837
[56] Zhang X X, Yan Q Z, Yang C T, Wang T N, Xia M and Ge C C 2016 *Rare Metals* **35** 566
[57] Fikar J and Schaeublin R 2007 *Nucl. Instrum. Meth. B.* **255** 27
[58] You Y W, Kong X S, Wu X B, Liu C S, Chen J L and Luo G N 2017 *Nucl. Fusion* **57** 016006
[59] Heinola K, Djurabekova F and Ahlgren T 2018 *Nucl. Fusion* **58** 026004
[60] Gonzalez C and Iglesias R 2014 *J. Mater. Sci.* **49** 8127
[61] https://cascadesdb.org/
[62] Norgett M, Robinson M and Torrens I 1975 *Nucl. Eng. Des.* **33** 50